Herschel[*]-ATLAS/GAMA: SDSS cross-correlation induced by weak lensing

J. González-Nuevo,[1,2†] A. Lapi,[2,3] M. Negrello,[4] L. Danese,[2] G. De Zotti,[2,4]
S. Amber,[5] M. Baes,[6] J. Bland-Hawthorn,[7] N. Bourne,[8,9] S. Brough,[10]
R. S. Bussmann,[11] Z.-Y. Cai,[2] A. Cooray,[12] S. P. Driver,[13,14] L. Dunne,[15]
S. Dye,[8] S. Eales,[16] E. Ibar,[17] R. Ivison,[9] J. Liske,[18] J. Loveday,[19]
S. Maddox,[15] M. J. Michałowski,[9] A. S. G. Robotham,[13] D. Scott,[20]
M. W. L. Smith,[16] E. Valiante[16] and J.-Q. Xia[21]

Affiliations are listed at the end of the paper

ABSTRACT

We report a highly significant ($>10\sigma$) spatial correlation between galaxies with $S_{350\,\mu m} \geq 30$ mJy detected in the equatorial fields of the *Herschel* Astrophysical Terahertz Large Area Survey (H-ATLAS) with estimated redshifts $\gtrsim 1.5$, and Sloan Digital Sky Survey (SDSS) or Galaxy And Mass Assembly (GAMA) galaxies at $0.2 \leq z \leq 0.6$. The significance of the cross-correlation is much higher than those reported so far for samples with non-overlapping redshift distributions selected in other wavebands. Extensive, realistic simulations of clustered sub-mm galaxies amplified by foreground structures confirm that the cross-correlation can be explained by weak gravitational lensing ($\mu < 2$). The simulations also show that the measured amplitude and range of angular scales of the signal are larger than can be accounted for by galaxy–galaxy weak lensing. However, for scales $\lesssim 2$ arcmin, the signal can be reproduced if SDSS/GAMA galaxies act as signposts of galaxy groups/clusters with halo masses in the range $10^{13.2}$–$10^{14.5}$ M$_\odot$. The signal detected on larger scales appears to reflect the clustering of such haloes.

Key words: methods: statistical – cosmology: observations – large-scale structure of Universe – infrared: galaxies.

1 INTRODUCTION

Light rays coming from a distant source are deflected by the foreground gravitational field. This, on the one hand, stretches the area of a given sky region, thus decreasing the surface density of sources and, on the other hand, magnifies the background sources, increasing their chances of being included in a flux-limited sample. The net effect, termed 'magnification bias', is extensively described in the literature (see e.g. Schneider, Ehlers & Falco 1992). It implies that an excess/decrease of background sources from a flux-limited sample will be found in the vicinity of matter overdensities (Bartelmann & Schneider 1993; Moessner & Jain 1998; Scranton et al. 2005). The amplitude of the excess increases with the slope of the

background source number counts. Thus, gravitational lensing constitutes a direct probe of the cosmic gravitational field. The most dramatic manifestations of lensing, called 'strong lensing', which includes multiple images, arcs or 'Einstein rings', are rare however. These manifestations show up on angular scales of arcseconds and provide information on high-density structures such as galaxies or galaxy clusters. The lower density structures, which include most of the mass in the Universe, nevertheless, can still produce observable effects via 'weak lensing'. The magnification bias due to weak lensing modifies the galaxy angular correlation function, because the observed images do not coincide with true source locations (Gunn 1967; Kaiser 1992; Moessner, Jain & Villumsen 1998; Loverde, Hui & Gaztañaga 2008), but the effect is generally small and difficult to single out. An unambiguous manifestation of weak lensing is the cross-correlation between two source samples with non-overlapping redshift distributions. The occurrence of such correlations has been tested and established in several contexts: 8σ detection of cosmic magnification from the galaxy–quasar cross-correlation function (Scranton et al. 2005); a simultaneous detection of gravitational

magnification and dust reddening effects due to galactic haloes and large-scale structure (galaxy–quasar cross-correlation; Ménard et al. 2010); and a 7σ detection of a cross-correlation signal between $z \sim$ 3–5 Lyman-break galaxies and *Herschel* sources (Hildebrandt et al. 2013) among others. See also Bartelmann & Schneider (2001) and references therein.

Since gravitational magnification decreases the effective detection limit, the amplitude of the magnification bias increases with increasing steepness of the number counts of background sources, and is then particularly large at sub-mm wavelengths, where the counts are extremely steep (Clements et al. 2010; Oliver et al. 2010). As demonstrated by Negrello et al. (2010), this property can be used to effectively identify strongly lensed galaxies in the sub-mm band, opening a new era of gravitational lensing studies (Ivison et al. 2010; Swinbank et al. 2010; Conley et al. 2011; Cox et al. 2011; Bussmann et al. 2012, 2013; Fu et al. 2012; Harris et al. 2012; Wardlow et al. 2013). At the same time, for a survey covering a sufficiently large area the counteracting effect on the solid angle is small (Jain & Lima 2011). A substantial fraction of galaxies detected by deep large area *Herschel* surveys at 250, 350 and 500 µm with the Spectral and Photometric Imaging Receiver (SPIRE; Griffin et al. 2010) reside at $z \gtrsim 1.5$ (Amblard et al. 2010; Lapi et al. 2011; Pearson et al. 2013) and therefore constitute an excellent background sample for the Sloan Digital Sky Survey (SDSS) galaxies, which are located at $z \lesssim 0.8$ (with a median redshift of $z \sim 0.1$).

A first attempt at measuring lensing-induced cross-correlations between *Herschel*/SPIRE galaxies and low-z galaxies was carried out by Wang et al. (2011), who found convincing evidence of the effect. The analysis can now be made with much better statistics, thanks to the availability of catalogues of *Herschel*/SPIRE sources covering much larger areas, new releases of SDSS data and the spectroscopic measurements of the Galaxy And Mass Assembly (GAMA; Driver et al. 2011) with many more galaxy spectra than SDSS for those areas (Baldry et al. 2010). Such an improved study is the subject of this paper. The paper is structured as follows. In Section 2, we describe the selection of background and foreground samples. In Section 3, we present our estimates of the auto- and cross-correlation functions, while in Section 4 we describe the simulations we have carried out to interpret the results. The main results are summarized and discussed in Section 5. A complementary analysis using cross-correlation measurements with different selections of both foreground and background samples, aimed at constraining the redshift distribution of the background sources, has been carried out by Schneider et al. (in preparation). In addition, an analysis of the effect of lensing on the identification of sub-millimetre galaxies in the *Herschel* Astrophysical Terahertz Large Area Survey (H-ATLAS; Eales et al. 2010) has been carried out by Bourne et al. (in preparation).

Throughout the paper, we adopt a flat ΛCDM cosmology with matter density $\Omega_m = 0.32$, $\Omega_\Lambda = 0.68$ and Hubble constant $h = H_0/100\,\mathrm{km\,s^{-1}\,Mpc^{-1}} = 0.67$ (Planck Collaboration 2013).

2 SAMPLE SELECTION

We have selected our background sample from the catalogue of sources detected in the three H-ATLAS equatorial fields, covering altogether $\simeq 161\,\mathrm{deg^2}$. The H-ATLAS is the largest area extragalactic survey carried out by the *Herschel* space observatory (Pilbratt et al. 2010), covering $\sim 550\,\mathrm{deg^2}$ with PACS (Poglitsch et al. 2010) and SPIRE (Griffin et al. 2010) instruments between

100 and 500 µm. Details of the H-ATLAS map-making, source extraction and catalogue generation can be found in Ibar et al. (2010), Pascale et al. (2011), Rigby et al. (2011), Maddox et al. (in preparation) and Valiante et al. (in preparation).

To extract high-redshift ($z \geq 1.5$) candidate galaxies we have adopted, similar to Lapi et al. (2011), the following criteria: (i) 250 µm flux density $S_{250} \geq 35$ mJy; (ii) no SDSS counterpart with reliability $R > 0.8$, as determined by Smith et al. (2011); and (iii) $\geq 3\sigma$ detection at 350 µm. We added the further constraint $S_{350} \geq 30$ mJy to facilitate comparison with the simulations described in Section 4. As pointed out by Lapi et al. (2011) requirement (ii) introduces a bias against H-ATLAS sources that are strongly lensed by SDSS galaxies closely aligned with them (which may be misinterpreted as their optical counterparts). Such objects are rare, however, and their loss is irrelevant for the purposes of this paper.

Next, we have estimated the photometric redshifts of the selected galaxies by means of a minimum χ^2 fit of a spectral energy distribution (SED) template to the PACS (which are mostly upper limits) and SPIRE data. As shown by Lapi et al. (2011) and González-Nuevo et al. (2012), a good template is the SED of SMM J2135$-$0102 ('The Cosmic Eyelash' at $z = 2.3$; Ivison et al. 2010; Swinbank et al. 2010). A comparison with spectroscopic redshifts has shown that the use of this template does not introduce any systematic offset and has reasonably low rms error (median $\Delta z/(1 + z) \equiv (z_{phot} - z_{spec})/(1 + z_{spec}) = -0.002$, with a dispersion of 0.115 and no outliers; González-Nuevo et al. 2012). Similar conclusions were obtained by Pearson et al. (2013), confirming our approach. Our background sample comprises all sources with photometric redshift $z \geq 1.5$, 26 630 sources in total. The distribution of selected sources on the plane of the sky for the 9 h H-ATLAS fields (one-third of the total equatorial survey) is shown, as an example, in Fig. 1. The area covered is made of four partially overlapping regions (hereafter 'tiles'), each of about 3.8×3.8. The estimated redshift distribution of selected sources in one of the tiles is shown in Fig. 2. Similar redshift distributions are found with the other tiles. The accuracy of our photometric redshift estimates is enough to avoid any overlap with foreground sources, for which we require $z \leq 0.6$.
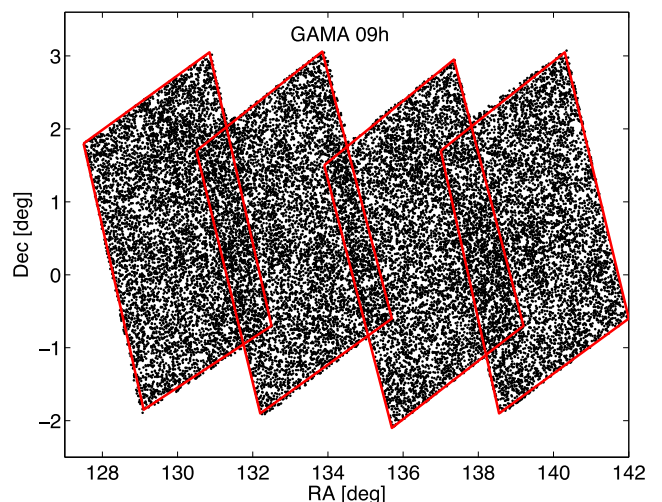

Figure 1. Distribution of selected H-ATLAS sources in the 9 h equatorial field (one-third of the total equatorial regions). The field is made of four partially overlapping areas, referred to as 'tiles'.
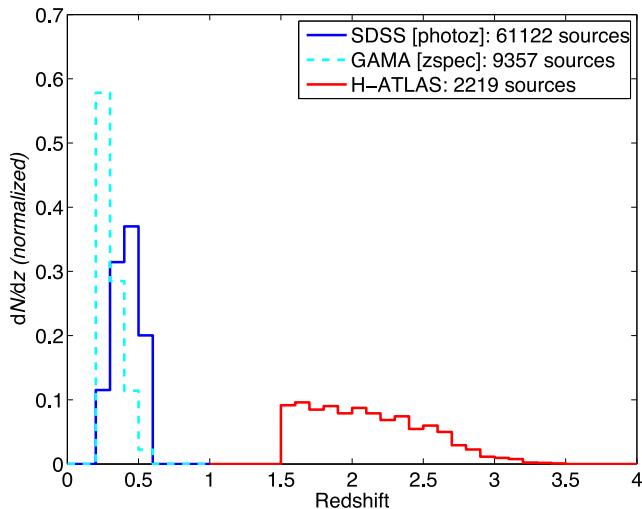
Figure 2. Redshift distributions of the background H-ATLAS sample (red histogram), the SDSS photometric sample (in blue) and the GAMA spectroscopic one (in cyan) for one of the tiles.

Figure 3. Distribution of the *zspec* sample sources in the 12 tiles. The 24 mini-tiles with green boundaries have obvious coverage 'holes' and were not used in the analysis. For clarity, only the first 2000 randomly selected galaxies per tile are shown.

Our main foreground sample is extracted from the Ninth Data Release of the SDSS (Ahn et al. 2012)[1] and comprises all galaxies in the H-ATLAS fields with $r < 22$ and *photometric* redshifts in the range $0.2 \leq z \leq 0.6$ (hereafter the *photoz* sample). Following the results of Lapi et al. (2012), we do not expect a relevant gravitational lensing effect for galaxies at $z < 0.2$, while their much higher number would slow down our calculations. On the other hand, the number of galaxies at $z > 0.6$ is so relatively small that they cannot produce any important statistical contribution to our results. We prefer to increase the redshift gap between the foreground–background samples in order to minimize the potential cross-contamination (see Section 3.3). We did not impose any constraint on the quality of the photometric redshift, to avoid biasing the sample towards lower redshift galaxies that are less effective as gravitational lenses. Taking into account that galaxies with low stellar masses, $M_\star \lesssim 10^{10.5}\,M_\odot$, produce negligible amplifications for the angular scales considered in our analysis, we have arbitrarily set a lower limit of $M_\star > 10^{10.4}\,M_\odot$ (see Section 4 for more details about mass estimation). In addition, we have also imposed an upper limit to the r-band luminosity, $L_r < 10^{11.6}\,L_\odot$, in order to remove sources with anomalously bright r-band luminosities, which are probably due to overestimates of the photometric redshifts ($\lesssim 0.3$ per cent of the total). At about this limit we have noticed an excess of galaxies with respect to the luminosity function derived by Bernardi et al. (2013) (see Section 4). The sample comprises $\sim 5 \times 10^4$ galaxies per tile, i.e. 686 333 galaxies in total. The redshift distribution for one of the tiles is shown by the blue histogram in Fig. 2. The median value is $z_{\rm phot, med} = 0.42$.

Accurate redshift measurements of the foreground sources are important to carry out realistic simulations of the effect of the gravitational lensing, which is related to the relative angular diameter distances between the observer, the lens and the source. On account of that, we have also defined a spectroscopic sample (hereafter the *zspec* sample) drawn from the GAMA II spectroscopic survey (Driver et al. 2009, Liske et al., in preparation). As a result of the coordination of the two surveys, there is substantial overlap among survey regions of H-ATLAS and GAMA. In particular, both surveys
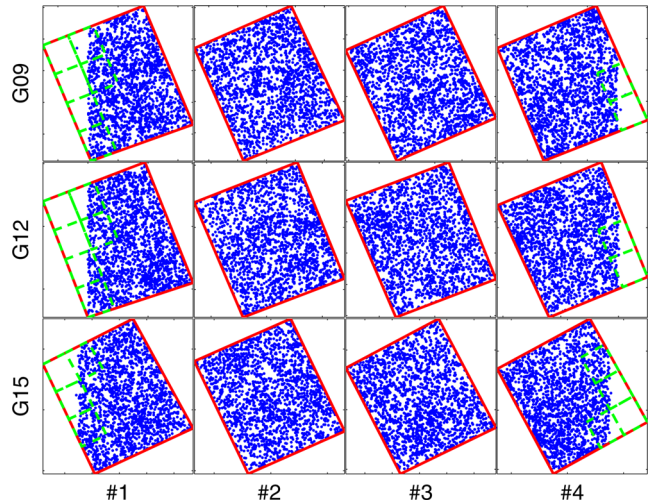
observed three equatorial regions at 9, 12 and 14.5 h (referred to as G09, G12 and G15, respectively). The GAMA II equatorial survey regions are $12° \times 5°$ in size, and were surveyed down to a limit of $r < 19.8$ mag. For our *zspec* sample, we select all GAMA II galaxies (from TilingCatv40) with reliable redshift measurements, which were made with a new fully automatic redshift code (Baldry et al. 2014), and $0.2 < z < 0.6$. This sample is smaller than the *photoz* one. It comprises $\simeq 9000$ galaxies per tile, i.e. 101 514 galaxies in total. Their median redshift, $z_{\rm spec, med} = 0.28$ is significantly lower than for the *photoz* sample, as shown by the cyan histogram in Fig. 2. Note that the magnification is far less sensitive to errors in the photometric redshifts of background sources, $\sigma_z \simeq 0.115(1 + z)$, since they have a small effect on the ratios of observer–source/lens–source angular diameter distance ratios.

A check of the distribution of galaxies in the *zspec* sample has shown that its coverage does not exactly match the H-ATLAS one, as illustrated in Fig. 3. To cure this, as well as to minimize the possible sample variance effect, we have divided each tile into 16 equal area mini-tiles (with green boundaries shown in Fig. 3) and we have excluded from further analysis the 24 mini-tiles with only a partial coverage. The *photoz* sample is immune to this problem, as illustrated in Fig. 4.

3 CORRELATION FUNCTIONS

3.1 Autocorrelation functions

The angular (auto)correlation function, $w(\theta)$, is a measure of the probability, in excess of the expectation for a Poisson distribution, of finding a galaxy within each of two infinitesimal solid angles separated by an angle θ, $P(\theta) = N[1 + w(\theta)]$, where N is the mean surface density of galaxies. We have computed $w(\theta)$ for the background and foreground samples using the Landy & Szalay (1993) estimator

$$w(\theta) = \frac{DD(\theta) - 2DR(\theta) + RR(\theta)}{RR(\theta)}, \qquad (1)$$

where $DD(\theta)$ is the number of unique pairs of real sources with separation θ, $DR(\theta)$ is the number of unique pairs between the real
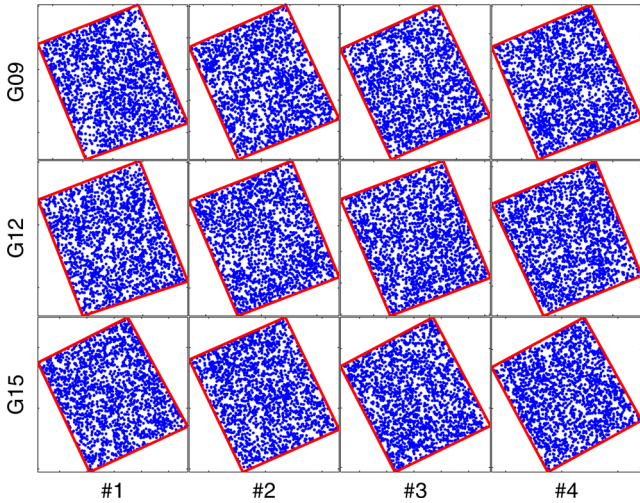
Figure 4. Distribution of the *photoz* sample sources in the 12 tiles. For clarity, only the first 2000 randomly selected galaxies per tile are shown.
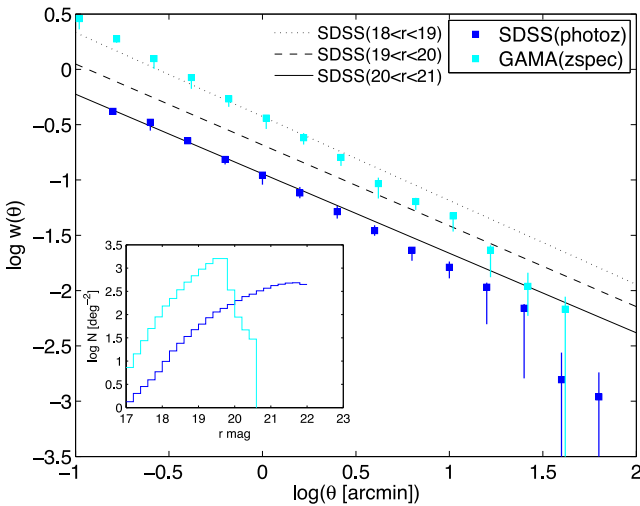

Figure 5. Autocorrelation function of our foreground samples compared with determinations of the best-fitting power laws using the full SDSS catalogue, split into magnitude intervals (Connolly et al. 2002; Wang, Brunner & Dolence 2013). The inset shows the distributions of *r*-band magnitudes for the two samples.

catalogue and a mock sample of sources with random positions, and $RR(\theta)$ is the number of unique pairs in the random source catalogue.

We computed the $w(\theta)$ of SDSS/GAMA galaxies for each tile (in order to determine it on scales of up to $\sim 1°$, not possible with the mini-tiles) and plotted in Fig. 5 the median values and the associated uncertainties estimated using the 'median statistics' of Gott et al. (2001). Median statistics lead to results that are quite similar and almost as constraining as χ^2 likelihood methods, but with somewhat more robustness since they do not assume Gaussianity of the errors or that their magnitudes are known. If we make N independent measurements M_i, where $i = 1, \ldots, N$, the probability that exactly n of the N measurements are higher than the true median is given by the binomial distribution, $P = 2^{-N}N!/[n!(N-n)!]$. Thus, if the measurements are ranked by value, such that $M_j > M_i$ for $j > i$, then the probability that the true median lies between M_i and M_{i+1} is

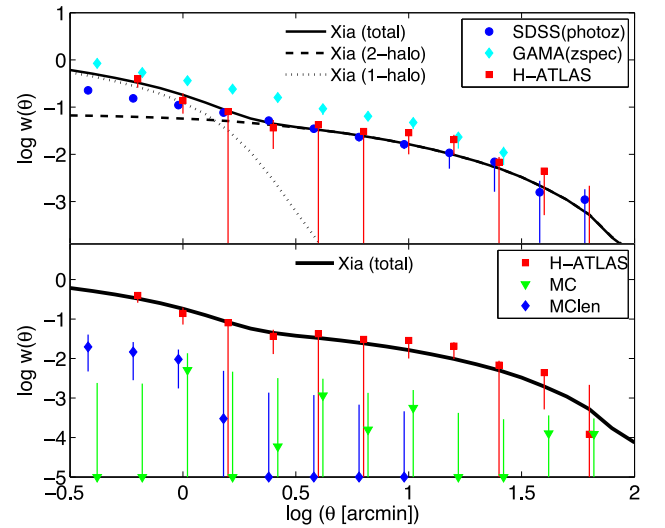$$P = \frac{2^{-N}N!}{[i!(N-i)!]}, \tag{2}$$

Figure 6. Top panel: autocorrelation functions of the H-ATLAS sample (red squares) and of the SDSS ones (blue squares, photometric; cyan squares, spectroscopic). Black lines show the expectations for the Xia et al. (2012) model for the background sources (dotted line, 1-halo term; dashed line, 2-halo term; solid line, total). Bottom panel: measured autocorrelation function of the H-ATLAS sample (red squares) compared with the expected contribution from weak lensing using the *zspec* sample and assuming that galaxies are signposts of groups of galaxies/cluster haloes (blue diamonds), based on ∼4500 Monte Carlo simulations (see the text for more details). The green upper limits come from ∼4500 Monte Carlo simulations of random distributions. The black solid line is the same as in the upper panel.

therefore providing a method for obtaining the confidence limits.

Our estimate for the photometric catalogue has low uncertainties and is in line with previous determinations carried out for several intervals of *r*-band magnitudes using the full SDSS catalogue (Connolly et al. 2002; Wang et al. 2013), taking into account that our sample is dominated by sources with $r \sim 21$. As shown in the inset of Fig. 5, the *zspec* sample is more weighted towards brighter sources ($r \leq 19$) due to an obvious selection bias. In agreement with SDSS autocorrelation results, the (magnitude limited) *zspec* sample is more clustered than the *photoz* one.

The angular (auto)correlation function of our background sample is shown in Fig. 6 (red filled squares). The computed autocorrelation was limited to angular scales ≳30 arcsec to avoid the potential bias caused by the resolution of the instruments (FWHM ∼ 18 and 25 arcsec for the 250 and 350 μm bands, respectively; Rigby et al. 2011). In the top panel of Fig. 6, the $w(\theta)$ of the background sources is compared with those of the foreground samples, as well as with the prediction of the Xia et al. (2012) best-fitting model. This model investigated the clustering of sub-millimetre galaxies in a self-regulated baryon collapse scenario by combining the physical evolutionary model for protospheroid galaxies of Granato et al. (2004) and an independent halo occupation distribution analysis. The cosmic infrared background power spectra at wavelengths from 250 μm to 2 mm measured by *Planck*, *Herschel*, South Pole Telescope and Atacama Cosmology Telescope experiments (see references in Xia et al. 2012) were fitted using the halo model with only two free parameters: the minimum halo mass; and the power-law index of the mean occupation function of satellite galaxies. The prediction shown in Fig. 6 (black lines) was computed adopting the redshift distribution of Fig. 2, without any adjustment of the parameters. The consistency between the model and the data is

excellent. The signal is clearly detected up to scales $\gtrsim 50$ arcmin; it is dominated by the 2-halo term on scales above $\simeq 2$ arcmin and by the 1-halo term on smaller scales. The lower panel will be commented upon in Section 4.

3.2 Cross-correlation functions

The cross-correlation function of two population of sources is the fractional excess probability, relative to a random distribution, of finding a source of Population 1 and a source of Population 2, respectively, within infinitesimal solid angles separated by an angle θ (Peebles 1980). We have computed the cross-correlation between our background and foreground samples using a modified version of the Landy & Szalay (1993) estimator (Herranz 2001)

$$w_{\text{cross}}(\theta) = \frac{D_1 D_2 - D_1 R_2 - D_2 R_1 + R_1 R_2}{R_1 R_2}, \qquad (3)$$

where $D_1 D_2$, $D_1 R_2$, $D_2 R_1$ and $R_1 R_2$ are the normalized data1-data2, data1-random2, data2-random1 and random1-random2 pair counts for a given separation θ (see Blake et al. 2006, for a discussion of different estimators of $w_{\text{cross}}(\theta)$).

We have followed the same procedure as in the autocorrelation case by computing the angular cross-correlation function, but this time for each of the 192 mini-tiles, and estimating the median values and the associated uncertainties using the 'median statistics' of Gott et al. (2001). Use of this procedure attempts to minimize the sample variance effect.

The measured angular cross-correlations between the foreground and background samples are shown in Fig. 7. Unlike the autocorrelation case, the small angular scale limit is dictated by the H-ATLAS positional error (relatively to which the SDSS error is negligibly
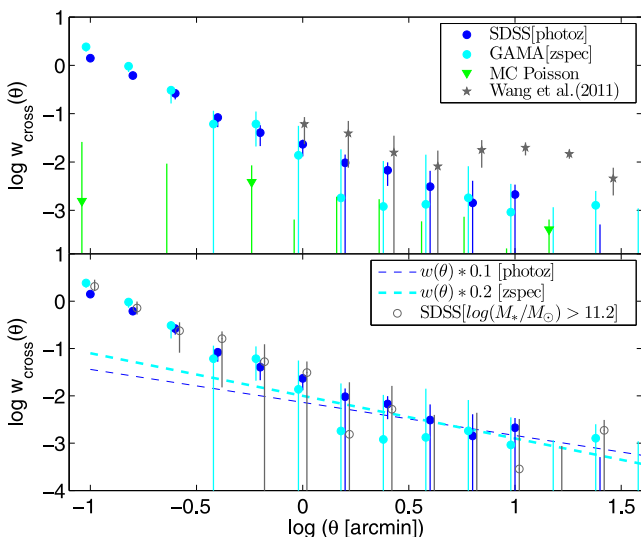

Figure 7. Top panel: cross-correlation between the H-ATLAS sample and the photometric and spectroscopic foreground samples (blue and cyan circles, respectively). Measurements from Wang et al. (2011) are also plotted for comparison (grey stars). The green upper limits are the result of ~2000 realistic Monte Carlo simulations, not accounting for the effect of lensing. Such simulations were made to check our procedure and to further illustrate the significance of the detected cross-correlation signal. Bottom panel: comparison of the measured cross-correlations with the autocorrelation functions of the photometric and spectroscopic foreground samples, scaled down by a factor of ~10 (blue dashed line) and ~20 (cyan dashed lines), respectively. The cross-correlation between the H-ATLAS sample and the photometric foreground sample, limited to $\log(M_\star/M_\odot) > 11.2$, is also shown.

small) whose rms value at $250\,\mu\text{m}$ is ~2.4 arcsec for 5σ sources (Rigby et al. 2011; Smith et al. 2011). To be conservative, we have limited our computations to angular scales $\gtrsim 6$ arcsec, greater than twice the H-ATLAS positional error. Our results are in broad agreement with those of Wang et al. (2011), although we do not confirm the strong signal reported by them on scales of tens of arcmin. The median values, uncertainties and additional statistical information on the cross-correlation results for both foreground samples can be found in Tables 1 and 2, where we also give the probability, from

Table 1. Measured cross-correlation between the H-ATLAS background sample and the photometric foreground galaxies, compared with the random source distribution case (estimated from ~2000 Monte Carlo simulations).

$\log\theta$ (arcmin)	Signal ($\pm$95% CL)	Random ($\pm$95% CL)	$\log p^a$
−1.0	$1.4400^{+0.2200}_{-0.1500}$	$-0.0197^{+0.0302}_{-0.0440}$	−77.9
−0.8	$0.6480^{+0.0530}_{-0.1090}$	$0.0112^{+0.0165}_{-0.0238}$	−62.6
−0.6	$0.2420^{+0.0400}_{-0.0440}$	$-0.0072^{+0.0116}_{-0.0113}$	−33.1
−0.4	$0.0758^{+0.0195}_{-0.0328}$	$-0.0027^{+0.0070}_{-0.0061}$	−8.2
−0.2	$0.0348^{+0.0177}_{-0.0124}$	$-0.0033^{+0.0044}_{-0.0039}$	−7.0
0.0	$0.0236^{+0.0092}_{-0.0098}$	$0.0013^{+0.0032}_{-0.0038}$	−4.8
0.2	$0.0067^{+0.0076}_{-0.0083}$	$-0.0010^{+0.0019}_{-0.0021}$	−2.4
0.4	$0.0061^{+0.0042}_{-0.0025}$	$0.0003^{+0.0012}_{-0.0015}$	−3.4
0.6	$0.0021^{+0.0045}_{-0.0049}$	$-0.0001^{+0.0008}_{-0.0008}$	−4.1
0.8	$0.0017^{+0.0013}_{-0.0030}$	$-0.0001^{+0.0005}_{-0.0008}$	−3.8
1.0	$0.0016^{+0.0015}_{-0.0022}$	$0.0000^{+0.0003}_{-0.0004}$	−5.6
1.2	$-0.0013^{+0.0013}_{-0.0013}$	$-0.0003^{+0.0002}_{-0.0002}$	−2.4
1.4	$-0.0010^{+0.0016}_{-0.0011}$	$0.0001^{+0.0001}_{-0.0001}$	−4.8

^{a}Here, p is the probability, from the Kolmogorov–Smirnov test, that the measured median $w_{\text{cross}}(\theta)$ is obtained from the random source distribution.
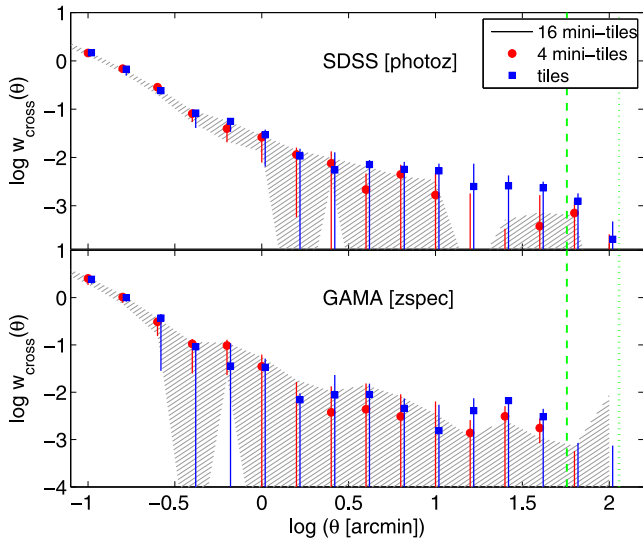
Table 2. Measured cross-correlation between the H-ATLAS background sample and the spectroscopic foreground galaxies, compared with the random source distribution case (estimated from ~2000 Monte Carlo simulations).

$\log\theta$ (arcmin)	Signal ($\pm$95% CL)	Random ($\pm$95% CL)	$\log p^a$
−1.0	$2.4050^{+0.3650}_{-0.4850}$	$0.0000^{+0.0001}_{-0.0001}$	−37.9
−0.8	$0.9585^{+0.1715}_{-0.2335}$	$-0.0755^{+0.0166}_{-0.0170}$	−25.2
−0.6	$0.3095^{+0.0735}_{-0.1315}$	$-0.0189^{+0.0090}_{-0.0101}$	−8.9
−0.4	$0.0655^{+0.0311}_{-0.0630}$	$-0.0085^{+0.0065}_{-0.0073}$	−3.3
−0.2	$0.0641^{+0.0459}_{-0.0485}$	$-0.0029^{+0.0038}_{-0.0047}$	−2.9
0.0	$0.0163^{+0.0394}_{-0.0341}$	$0.0008^{+0.0019}_{-0.0029}$	−1.9
0.2	$0.0014^{+0.0151}_{-0.0174}$	$-0.0004^{+0.0020}_{-0.0018}$	−0.1
0.4	$-0.0010^{+0.0097}_{-0.0092}$	$-0.0005^{+0.0011}_{-0.0010}$	−0.6
0.6	$0.0012^{+0.0107}_{-0.0078}$	$-0.0008^{+0.0006}_{-0.0006}$	−2.3
0.8	$0.0023^{+0.0067}_{-0.0071}$	$0.0001^{+0.0004}_{-0.0004}$	−2.5
1.0	$0.0004^{+0.0029}_{-0.0055}$	$0.0000^{+0.0003}_{-0.0003}$	−3.0
1.2	$-0.0006^{+0.0019}_{-0.0033}$	$-0.0000^{+0.0002}_{-0.0002}$	−1.1
1.4	$0.0011^{+0.0016}_{-0.0022}$	$-0.0000^{+0.0001}_{-0.0001}$	−2.7

^{a}Here, p is the probability, from the Kolmogorov–Smirnov test, that the measured median $w_{\text{cross}}(\theta)$ is obtained from the random source distribution.

Figure 8. Observed cross-correlation between the H-ATLAS sample and the *photoz* (top panel) and *zspec* (bottom panel) samples (grey hatched area; dividing each tile in 16 mini-tiles), compared with the measured ones dividing each tile into 4 mini-tile (red circles) or using the whole tiles (blue squares). The green dashed and dotted lines indicate the typical sizes of the 16 and 4 mini-tiles, respectively.

the Kolmogorov–Smirnov test, that the measured median $w_{\mathrm{cross}}(\theta)$ is obtained from a random source distribution. It is clear from the table that the significance of the signal from the *photoz* sample is very high. This is in fact the best detection of lensing-induced cross-correlation reported so far.

The limited number of foreground galaxies slightly diminishes the significance of the signal derived from the *zspec* sample. However, the similarity between the signal from both foreground samples makes us confident that potential systematic uncertainties in the photometric redshift estimation are not an issue.

Below 20–30 arcmin the measured cross-correlation is almost independent of the mini-tile size used (see Fig. 8). At larger angular scales the observed signal, using 16 or 4 mini-tiles per tile, are biased low. However, we decided to continue dividing the tiles in 16 smaller areas due to the lower uncertainties at angular scales below ∼3 arcmin.

The bottom panel of Fig. 7 compares the measured cross-correlations with the autocorrelation functions of the photometric and spectroscopic foreground samples, scaled down by factors of ∼10 and ∼20, respectively. These factors correspond to the probability of lensing with moderate amplifications, $\mu < 2$, for the different median redshifts of the samples (Lapi et al. 2012). This comparison suggests that, above a few arcmin, the cross-correlation functions reflect the clustering properties of the foreground samples. We have investigated this possibility and, more generally, the interpretation of the cross-correlation signals by means of extensive simulations, described in Section 4.

Finally, we have checked that most of the cross-correlation signal for the *photoz* sample is produced by the most massive SDSS sources, $\log (M_\star/\mathrm{M}_\odot) > 11.2$ or $\log (M_\mathrm{h}/\mathrm{M}_\odot) \gtrsim 13.2$ (Fig. 7, grey circles). However, the lower number of such objects translates into a larger uncertainty in the measured signal.

3.3 Assessment of the potential cross-contamination

As discussed in detail in Lapi et al. (2011), a cold observed SED may be associated either with a low-z cirrus-dominated galaxy or to a redshifted warm galaxy, introducing a potential degeneracy. This problem can be overcome, however, because cold, low-z galaxies are only moderately obscured by dust (the cirrus optical depth cannot be very large), and are therefore relatively bright in the optical bands. For this reason, as described in Section 2, we removed from the background sample those sources that have an SDSS counterpart with reliability $R > 0.8$, even if this requirement introduces a bias against H-ATLAS strongly lensed sources. For the rest of the background sources, so far we have assumed that errors on photometric redshifts do not cause any overlap between background and foreground samples.

H-ATLAS sources with intermediate values of reliability, $0.1 < R < 0.8$ (i.e. that have a non-negligible probability of being SDSS/GAMA sources that we could have incorrectly considered as H-ATLAS sources at $z > 1.5$), constitute only ∼9 per cent of the background sample. In addition, the limiting colour used to separate elliptical from spiral galaxies ($g - r > 0.8$; Bernardi et al. 2010) increases with redshift, but remains approximately constant around $g - r \sim 1.5$ in the redshift range $0.2 < z < 0.6$, for typical elliptical SEDs. We have checked that ∼30 per cent of these sources have colours compatible with elliptical galaxies, $g - r > 1.5$, and therefore are expected to have sub-mm emission that is hardly detectable by *Herschel*.

For the other ∼70 per cent, following González-Nuevo et al. (2012), we have verified that the ratios between the r-band flux density and those at 350 and 500 µm are much higher than expected for spiral galaxies, or even for the median local starburst SED (Smith et al. 2012), both placed at $z = 0.6$. In fact, only ∼1 per cent of those sources, for the spiral SED, and ∼6 per cent, for the local starburst one, show compatible ratios. This means that the SDSS magnitudes of those sources are too faint to account for the optical and far-IR emissions at the same time, *if they have the cold far-IR SEDs observed for $z < 0.6$ galaxies with moderate star formation rates*. In other words, most of the remaining background sources have higher apparent far-IR to optical luminosity ratios than the spiral or Smith et al. (2012) galaxies, akin to those of sub-mm galaxies, and/or have colder far-IR colours. This implies that they must be at higher redshifts than those indicated by the optical/near-IR SEDs of their SDSS counterparts. Therefore, from this photometric analysis, we estimated that the fraction of SDSS/GAMA sources that we could have incorrectly considered as H-ATLAS sources at $z > 1.5$ is lower than $0.09 \times 0.6 \times 0.06 \sim 0.4$ per cent (for the median local starburst SED case).

A similar upper-limit, ∼1 per cent, is obtained if we consider the removed $R > 0.8$ sources as a rough indicator of the cross-contamination (remember that many strongly lensed galaxies fall in this category). The fraction of background sources with an $R > 0.8$ optical counterpart in the foreground sample is roughly 9 per cent. Of these sources, again only ∼9 per cent have apparent far-IR to optical luminosity ratios compatible with local starburst galaxies at $z < 0.6$.

A small part of the H-ATLAS area is covered by a very deep VLA survey of the Subaru Deep Field (Ivison et al. in preparation). We have used this survey to find very reliable ($R > 0.99$) radio counterparts for approximately 100 H-ATLAS sources. These sources have been preliminarily identified in deep optical/near-IR imaging (from the Subaru Deep Field) and high-quality photometric redshifts have been derived from these data. Of the 27 sources that satisfy the
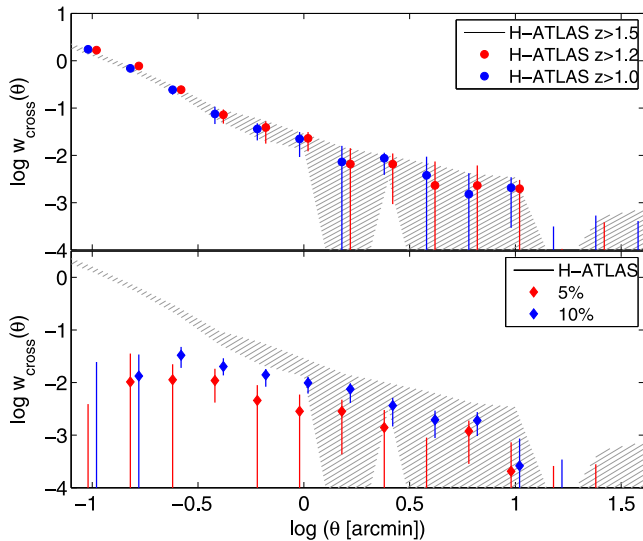
Figure 9. Top panel: estimated cross-correlation between the *photoz* sample and a background sample that extends to lower redshifts (red circles, 1.2 < z < 4.0; blue circles, 1.0 < z < 4.0). Bottom panel: potential cross-contamination inferred from simulations if 5 or 10 per cent of the background sources are considered as foreground galaxies (randomly selected in each case). In both panels, the grey hatched area corresponds to the observed cross-correlation between the H-ATLAS sample and the *photoz* sample.

parent sample selection criteria (see Section 2), 24 are at $z > 0.9$. Therefore, there is a maximum potential cross-contamination of ∼10 per cent, although probably much lower, because some of these three particular cases could be foreground galaxies acting as lenses (Allen et al. in preparation).

The H-ATLAS parent sample selection procedure produces a Gaussian-like redshift distribution peaked around $z \sim 2$, with a lower tail that extends to $z \sim 0.5$ (see fig. 4 of Lapi et al. 2011). By selecting only those sources with $z > 1.5$ we are minimizing the potential cross-contamination and maintaining the bulk of the sample at the same time. However, we can relax this minimum redshift in order to verify that, if an overlap exists, its cross-contamination effect in the measured cross-correlation signal is negligible. As shown in Fig. 9 (top panel), the measured signal remains almost the same, independent of the lower redshift limit used, hence confirming the non-overlap assumption.

Finally, we have used the simulations described in Section 4 to assess the potential cross-contamination produced by a non-negligible fraction of mismatched background versus foreground sources (see Fig. 9, bottom panel). In this particular set of simulations, a fraction of background sources are randomly selected and moved to the position of randomly selected foreground ones. The results show that an ∼10 per cent contamination by overlapping background/foreground sources is ruled out, because it would yield a far stronger cross-correlation signal on scales ≥1 arcmin than measured for our samples, yet falling short of accounting for the observed signal on smaller scales.

4 REALISTIC SIMULATIONS

In this paper, we focus on the measured cross-correlation signal between two different samples, without taking into account possible completeness issues or selection biases in the foreground samples. This decision, aimed at maximizing the number of sources in both samples, complicates the theoretical interpretation of the

measured signal. For this reason, we carried out realistic simulations of the background sources, using the actual information (position, photometry and redshift) for the foreground sources. With this approach, the potential statistical issues with the foreground sources are fully dealt with.

4.1 Simulation set-up and results

We have generated simulated three-dimensional distributions of background sources down to $S_{350} = 10$ mJy, drawing them from the redshift-dependent luminosity functions of un-lensed galaxies yielded by the Cai et al. (2013) model (which updates the model by Lapi et al. 2011, and reproduces the observed counts, after allowing for the effect of gravitational lensing). Since the cross-correlations are induced mainly by weak lensing, a flux density limit of 10 mJy is sufficient for the parent sample, given that the flux density limit of the background sample we want to simulate is 30 mJy. The clustering properties of the sources were generated using the software described in González-Nuevo, Toffolatti & Argüeso (2005), with the spatial correlation functions $\xi(r, z)$ given by the Xia et al. (2012) model. This model successfully reproduces the clustering properties of *Herschel* galaxies, as well as the power spectra of fluctuations of the cosmic infrared background measured by both *Planck* and *Herschel*. We performed typically 10 simulations per mini-tile.

Next, we have estimated the magnification of each background source by the foreground source closest to its line of sight, using the formalism of Lapi et al. (2012) that requires four ingredients: z_{lens}; z_{source}; halo mass of the lens, M_h; and angular separation between source and lens (triaxiality effects were neglected). The calculations were performed for several choices of the relation between M_h and the rest-frame r-band luminosity of the lens, using both the NFW (Navarro, Frenk & White 1996; Łokas & Mamon 2001) and classic singular isothermal sphere (SIS) density profiles. The flux densities of the background sources were updated, taking the gravitational amplification into account, and the simulated background sample was constructed by selecting sources with $S_{350} > 30$ mJy and $z \geq$ 1.5. For the foreground samples, we used either the real positions and redshifts of sources or we randomized the positions, keeping the measured or estimated redshifts the same.

As a preliminary test, we computed the cross-correlation between the simulated background sample and the foreground samples, ignoring the effect of lensing, in the same way as we did for real samples. As illustrated by the green points in the upper panel of Fig. 7, no significant correlation was found.

In the next set of simulations, we estimated M_h using the relationship with the r-band luminosity, L_r, derived by Shankar et al. (2006) for elliptical galaxies (galaxy–galaxy lensing). In this case, the chosen density profile of the foreground sources was the SIS one, and we allowed for strong-lensing. Two conclusions are immediately apparent (see green diamonds in the top panel of Fig. 10).

(i) A statistically significant cross-correlation appears on small scales, demonstrating that the observed signal is indeed due to gravitational lensing.

(ii) The cross-correlation due to galaxy–galaxy lensing falls rapidly on scales larger than ∼30 arcsec. Even on smaller scales it has an insufficient amplitude; therefore it cannot account for the detected signal.

The reason for the second result is illustrated in Fig. 11, showing that the gravitational amplification by galaxy-scale lenses is negligible on scales larger than 40–50 arcsec. Much more massive lenses, which also give stronger effects, must be advocated. This suggests
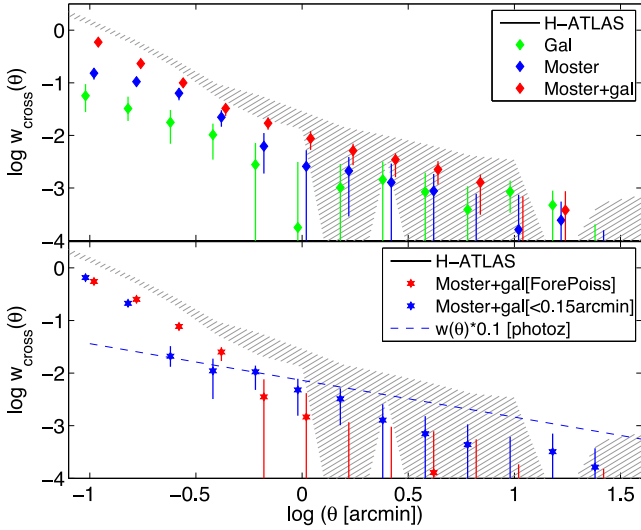
Figure 10. Top panel: observed cross-correlation between the H–ATLAS sample and the *photoz* samples (grey hatched area) compared with the one inferred from simulations of lensing by galactic haloes (green diamonds), by group/cluster haloes with NFW density profiles (magenta diamonds) and a combination of both (red diamonds). Bottom panel: effect of ignoring the clustering properties of foreground galaxies is illustrated by simulations of the effect of lensing by a random distribution of foreground galaxies ('Moster+gal' case; red stars). On the other hand, by limiting the direct effect of lensing to angular scales <0.15 arcmin, the recovered cross-correlation signal reflects the autocorrelation of the foreground galaxies (blue stars) above such scales. The blue dashed line shows the power-law representation of the autocorrelation of foreground sample, scaled down by a factor of 10. The grey hatched area shows the same observed cross-correlation as in the top panel.
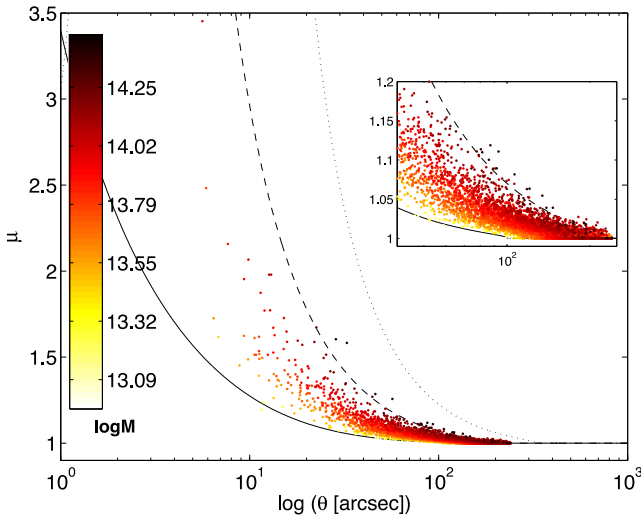
Figure 11. Gravitational amplifications of background sources as a function of angular distance and lens halo mass (see the colour scale on the left) obtained in the simulations of a single tile. The black lines correspond to a source at redshift $z_s = 2.5$ and lenses with $M_h = 3 \times 10^{13}$, 3×10^{14} and 10^{15} M$_\odot$ (solid, dashed and dotted lines, respectively), all at $z_{\rm lens} = 0.5$.

that galaxies in the foreground samples act as signposts for much more massive haloes, i.e. are typically the central galaxy of a group or cluster of galaxies.

To test this hypothesis, we have associated each galaxy with a halo mass, M_h, estimated in the following way. From the *r*-band
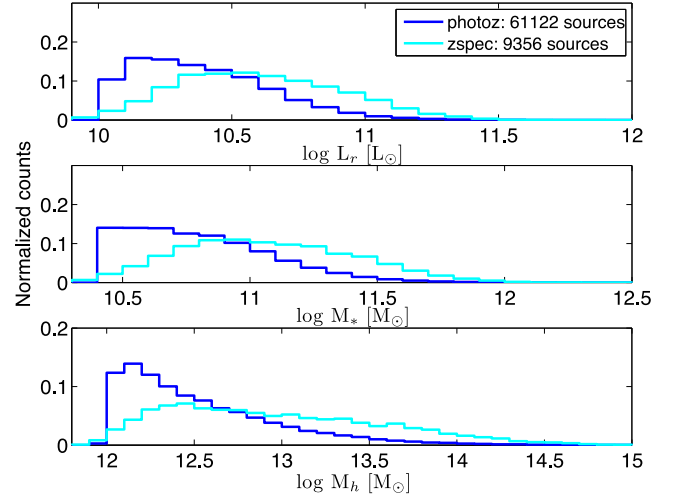
Figure 12. Normalized distribution of the estimated *r*-band luminosities, L_r, stellar masses, $M_\star$, and halo masses, M_h, of both foreground samples in a typical tile (see the text for more details).

luminosity, L_r, we estimated the stellar masses, $M_\star$, using a modified version of the luminosity–stellar mass relationship of Bernardi et al. (2003) and Shankar et al. (2006). We used a lower $(M/L)_0$ value than the original one by Bernardi et al. (2003), derived for the typical $(g - r) = 0.8$ elliptical colours, and we introduced an evolution correction factor (see Bell et al. 2003; Bernardi et al. 2010, for more details):

$$M_\star/L_r = 3 \times (L_r/10^{10.31})^{0.15} \times 10^{-0.19z}, \tag{4}$$

with $M_\star$ and L_r in M$_\odot$ and L$_\odot$, respectively. Then, we used the relationship between the stellar mass and halo mass from Moster et al. (2010, their equations 2 and 23–26 with the redshift-dependent parameters from table 7), which was determined imposing consistency between both mass functions. The normalized distribution of the estimated L_r, $M_\star$ and M_h for both foreground samples are shown in Fig. 12 for a typical tile. The luminosity, stellar mass and halo mass functions derived from these distributions are in agreement with the latest results (see Fig. 13, Moster et al. 2010; Bernardi et al. 2013, and references therein).

The upper panel of Fig. 10 shows the cross-correlation signal recovered by considering the weak lensing effect (we limited our analysis to angular separations >5 arcsec) produced by massive haloes with an NFW density profile. One might worry that associating such a massive halo with every foreground galaxy may be counting the same halo multiple times. Such events must be rare, however, because the typical comoving distance between a galaxy in the *photoz* sample and its nearest neighbour are ∼6.5 Mpc. Although the recovered signal is stronger than in the galaxy–galaxy lensing case, there is still a lack of power, probably indicating that our assumptions to build the simulations are not complex enough to completely reproduce the measured signal.

There are essentially two main ways to increase the number of background sources that appear, in projection, very close to the foreground ones, i.e. to increase the strength of the cross-correlation signal. First, we can adopt higher halo masses and/or higher numbers of deflectors, or satellites, per halo. However, increasing halo masses would lead to a density of massive haloes in excess of that obtained from *N*-body simulations. The second alternative makes reference to the fact that we have adopted the rather extreme assumption that each dark matter halo has either an NFW or an SIS density
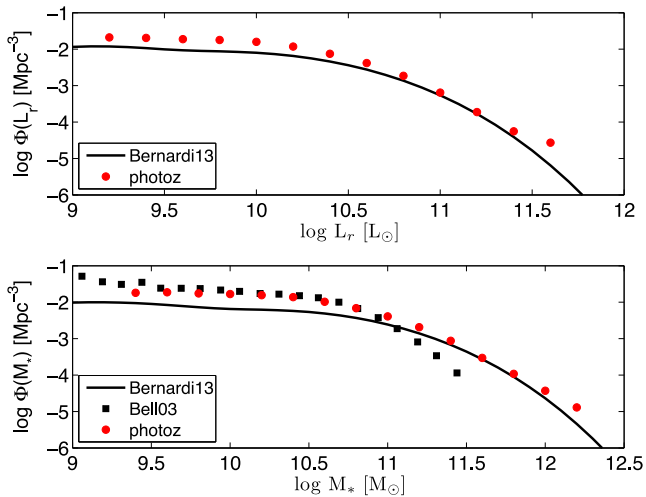
Figure 13. Luminosity function (top) and stellar mass function (bottom) estimated from the *photoz* sample (red circles). The luminosity function derived by Bernardi et al. (2013, black line, top panel) and the stellar mass functions from Bernardi et al. (2013, black line, bottom panel) and Bell et al. (2003, black squares, bottom panel) are shown for comparison.

profile centred at the position of the SDSS sources, without any sub-structure. Therefore, in order to understand the possible role of halo sub-structures, we have slightly modified the simulation set-up in the following way. We associate an SIS profile to each SDSS source with mass estimated from the Shankar et al. (2006) relationship. The SIS profile is centred on the SDSS galaxy. Then, we place an NFW mass profile 5 arcsec away from the SDSS source position, in a random direction, and estimate its mass using the Moster et al. (2010) relationship, as explained above. In other words, we have now assumed that the SDSS galaxies act as signposts of much more massive haloes, but are not located exactly at their centres.

The signal recovered using this set of simulations, *Moster+gal* (see Fig. 10), is in better agreement with the measured one. As expected from the halo model formalism (see e.g. Cooray & Sheth 2002), this last result confirms that sub-structures within a halo, i.e. satellites, have an important role to play in explaining the measured signal. Our simple approach is not able to completely reproduce the signal on scales below ~ 20–30 arcsec. However, more sophisticated simulations, beyond the scope of the current paper will be performed in a future work.

The direct effect of gravitational lensing by massive haloes (the 1-halo term) is not enough to account for the observed signal on arcmin scales. This was shown by repeating the simulations for the case of random distributions of both the background and foreground samples, so that any intrinsic autocorrelation is washed out. As a result (red stars in the bottom panel of Fig. 10), the statistical significance of the cross-correlations becomes marginal on scales larger than $\simeq 0.5$ arcmin. This proves that the signal on larger scales is due to the clustering of the large haloes (2-halo term; e.g. Cooray & Sheth 2002; Mandelbaum et al. 2013), i.e. it comes from the higher probability that background sources are amplified above the adopted flux density limit, 30 mJy, in the neighbourhood of the foreground deflectors. This interpretation is supported by the change in the slope of the cross-correlation function for $\theta \geq 1$ arcmin. It appears to reflect the autocorrelation function of the foreground sample, sketched in Fig. 10 by the blue dashed line (corresponding to its power-law representation with amplitude decreased by a factor of 10). This factor is probably related to the probability of lensing; for

the typical properties of foreground and background samples the factor is around ~ 10 per cent for $\mu \sim 1.5$ (Lapi et al. 2012). In fact, if we take into account the effect of lensing only for separations between background and foreground sources of less than 9 arcsec (blue stars in the bottom panel of Fig. 10), allowing for the possibility of strong lensing in this case, the recovered cross-correlation signal tends to reflect the autocorrelation of the foreground galaxies.

4.2 Further considerations

We conclude that the observed cross-correlation is the combination of two contributions. On sub-arcmin scales it comes directly from weak lensing of group/cluster sized haloes, while on larger scales it reflects the clustering of such haloes. This conclusion implies that the observed spatial distribution of the background sources is influenced by the clustering of foreground galaxies. The extreme case would be that the clustering properties of the background sample were completely due to the lensing effect. Therefore, we are led to ask, how much of the H-ATLAS sources clustering is intrinsic and not contributed by weak lensing effects? To answer this question, we have performed a set of 100 simulations per mini-tile, using the *zspec* foreground sample and intrinsically unclustered background galaxies. After lensing, the population indeed shows significant clustering, but at a level well below the observed one, <4 per cent (see Fig. 6, bottom panel). Strictly speaking, the lensing-induced clustering inferred from simulations is a lower limit to the real measurement, because simulations necessarily take into account only a subset of foreground galaxies. We expect, however, that the bulk of the effect comes from the redshift range covered by our foreground samples.

Previous measurements of the counts of sub-millimetre galaxies have been corrected for the effects of galaxy–galaxy lensing (Perrotta et al. 2002, 2003; Negrello et al. 2007, 2010; Paciga, Scott & Chapin 2009; Hezaveh & Holder 2011; Wardlow et al. 2013). However, the fact that the cross-correlation is dominated by lensing from group/cluster haloes suggests that substantial contributions may also come from these more massive haloes. As illustrated in Fig. 14, our simulations confirm that galaxy–galaxy strong lensing indeed dominates the effect on the counts, but a substantial contribution, at the brightest flux densities, may also come from much larger haloes.

As in the previous case, the lensing-induced clustering inferred from simulations is a lower limit to the real one, because simulations do not include all the foreground galaxies.

The AzTEC millimetre survey of the COSMOS field (Austermann et al. 2009; Aretxaga et al. 2011) showed an observed excess in number counts at 1.1 mm and a spatial correlation with the optical–IR galaxy density, which seem consistent with lensing of a background sub-millimetre galaxy population by foreground mass structures along the line of sight. Our measured cross-correlation signal, and, in particular, the weak lensing effect produced by foreground structures on the bright end of the source number counts, appear to confirm these findings.

5 CONCLUSIONS

We have reported a highly significant correlation between the spatial distribution of H-ATLAS galaxies with estimated redshift $\gtrsim 1.5$ and that of SDSS/GAMA galaxies at $0.2 \leq z \leq 0.6$. Extensive, realistic simulations have shown that the cross-correlation is explained by weak gravitational lensing. The much higher significance compared
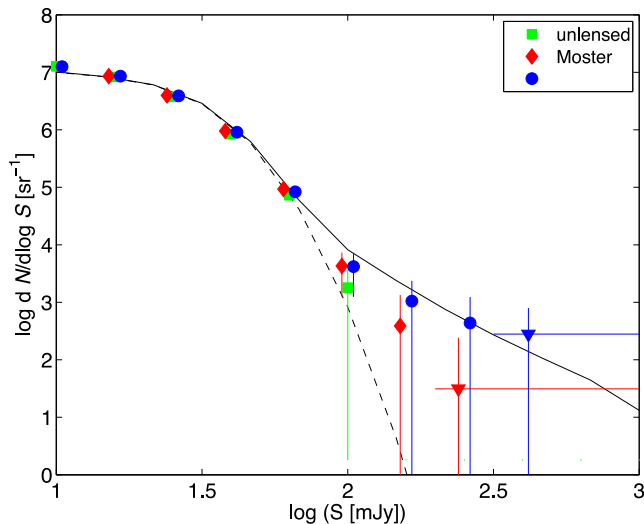
Figure 14. Gravitational lensing effect on the recovered source number counts at 350 μm from the Monte Carlo simulations (using the *zspec* sample). The black lines show the number counts from the Lapi et al. (2011) model, with (solid) and without (dashed) including the effect of gravitational lensing. The corresponding simulated counts are represented by the blue circles and by the green squares: the latter represent the unlensed counts, the former include the effect of galaxy–galaxy lensing. The red diamonds show the effect on the counts of weak lensing by group/cluster haloes. The triangle symbols at the bright end are upper limits.

to those reported so far is a result of the extreme steepness of the sub-mm source counts.

The simulations also show that the amplitude and the range of angular scales of the signal are larger than those that can be accounted for by galaxy–galaxy weak lensing. However, it can be reproduced, on sub-arcmin scales, if SDSS/GAMA galaxies act as signposts of galaxy groups/clusters with halo masses in the range $\sim 10^{13.2}$–$10^{14.5}$ M$_\odot$. The signal detected on larger scales appears to reflect the clustering of such haloes. Future work will try to extract quantitative astrophysical information about the dark matter haloes by comparing the measured cross-correlation signal with dedicated simulations, considering the distribution of sub-haloes and their densities, as well as observational constraints like angular resolution and sensitivity.

We have also investigated the effect of clustering of foreground galaxies on the observed angular correlation function of H-ATLAS galaxies. We find that lensing can indeed induce an apparent clustering of randomly distributed background galaxies, but the amplitude of the corresponding angular correlation function is at least a factor of 10 lower than observed.

Finally we find that, although haloes of group/cluster size are the dominant contributors to the cross-correlation between H-ATLAS and SDSS/GAMA galaxies, the gravitational magnification effects on counts of sub-mm sources are nevertheless dominated by galaxy–galaxy strong lensing.

ACKNOWLEDGEMENTS

REFERENCES

Ahn C. P. et al., 2012, ApJS, 203, 21
Amblard A. et al., 2010, A&A, 518, L9
Aretxaga I. et al., 2011, MNRAS, 415, 3831
Austermann J. E. et al., 2009, MNRAS, 393, 1573
Baldry I. K. et al., 2010, MNRAS, 404, 86
Baldry I. K. et al., 2014, MNRAS, 441, 2440
Bartelmann M., Schneider P., 1993, A&A, 268, 1
Bartelmann M., Schneider P., 2001, Phys. Rep., 340, 291
Bell E. F., McIntosh D. H., Katz N., Weinberg M. D., 2003, ApJS, 149, 289
Bernardi M. et al., 2003, AJ, 125, 1849
Bernardi M., Shankar F., Hyde J. B., Mei S., Marulli F., Sheth R. K., 2010, MNRAS, 404, 2087
Bernardi M., Meert A., Sheth R. K., Vikram V., Huertas-Company M., Mei S., Shankar F. et al., 2013, MNRAS, 436, 697
Blake C., Pope A., Scott D., Mobasher B., 2006, MNRAS, 368, 732
Bussmann R. S. et al., 2012, ApJ, 756, 134
Bussmann R. S. et al., 2013, ApJ, 779, 25
Cai Z.-Y. et al., 2013, ApJ, 768, 21
Clements D. L. et al., 2010, A&A, 518, L8
Conley A. et al., 2011, ApJ, 732, L35
Connolly A. J. et al., 2002, ApJ, 579, 42
Cooray A., Sheth R., 2002, Phys. Rep., 372, 1
Cox P. et al., 2011, ApJ, 740, 63

Driver S. P. et al., 2009, Astron. Geophys., 50, 050000
Driver S. P. et al., 2011, MNRAS, 413, 971
Eales S. et al., 2010, PASP, 122, 499
Fu H. et al., 2012, ApJ, 753, 134
González-Nuevo J., Toffolatti L., Argüeso F., 2005, ApJ, 621, 1
González-Nuevo J. et al., 2012, ApJ, 749, 65
Gott J. R., III, Vogeley M. S., Podariu S., Ratra B., 2001, ApJ, 549, 1
Granato G. L., De Zotti G., Silva L., Bressan A., Danese L., 2004, ApJ, 600, 580
Griffin M. J. et al., 2010, A&A, 518, L3
Gunn J. E., 1967, ApJ, 147, 61
Harris A. I. et al., 2012, ApJ, 752, 152
Herranz D., 2001, in Tran Thanh Van J., Mellier Y., Moniez M., eds, Cosmological Physics with Gravitational Lensing. EDP Sciences, Les Ulis, p. 197
Hezaveh Y. D., Holder G. P., 2011, ApJ, 734, 52
Hildebrandt H. et al., 2013, MNRAS, 429, 3230
Ibar E. et al., 2010, MNRAS, 409, 38
Ivison R. J. et al., 2010, A&A, 518, L35
Jain B., Lima M., 2011, MNRAS, 411, 2113
Kaiser N., 1992, ApJ, 388, 272
Landy S. D., Szalay A. S., 1993, ApJ, 412, 64
Lapi A. et al., 2011, ApJ, 742, 24
Lapi A., Negrello M., González-Nuevo J., Cai Z.-Y., De Zotti G., Danese L., 2012, ApJ, 755, 46
Łokas E. L., Mamon G. A., 2001, MNRAS, 321, 155
Loverde M., Hui L., Gaztañaga E., 2008, Phys. Rev. D, 77, 023512
Mandelbaum R., Slosar A., Baldauf T., Seljak U., Hirata C. M., Nakajima R., Reyes R., Smith R. E., 2013, MNRAS, 432, 1544
Ménard B., Scranton R., Fukugita M., Richards G., 2010, MNRAS, 405, 1025
Moessner R., Jain B., 1998, MNRAS, 294, L18
Moessner R., Jain B., Villumsen J. V., 1998, MNRAS, 294, 291
Moster B. P., Somerville R. S., Maulbetsch C., van den Bosch F. C., Macciò A. V., Naab T., Oser L., 2010, ApJ, 710, 903
Navarro J. F., Frenk C. S., White S. D. M., 1996, ApJ, 462, 563
Negrello M., Perrotta F., González-Nuevo J., Silva L., de Zotti G., Granato G. L., Baccigalupi C., Danese L., 2007, MNRAS, 377, 1557
Negrello M. et al., 2010, Science, 330, 800
Oliver S. J. et al., 2010, A&A, 518, L21
Paciga G., Scott D., Chapin E. L., 2009, MNRAS, 395, 1153
Pascale E. et al., 2011, MNRAS, 415, 911
Pearson E. A. et al., 2013, MNRAS, 435, 2753
Peebles P. J. E., 1980, The Large-Scale Structure of the Universe. Princeton Univ. Press, Princeton, NJ
Perrotta F., Baccigalupi C., Bartelmann M., De Zotti G., Granato G. L., 2002, MNRAS, 329, 445
Perrotta F., Magliocchetti M., Baccigalupi C., Bartelmann M., De Zotti G., Granato G. L., Silva L., Danese L., 2003, MNRAS, 338, 623
Pilbratt G. L. et al., 2010, A&A, 518, L1
Planck Collaboration, 2013, preprint (arXiv:1303.5076)
Poglitsch A. et al., 2010, A&A, 518, L2
Rigby E. E. et al., 2011, MNRAS, 415, 2336
Schneider P., Ehlers J., Falco E. E., 1992, Gravitational Lenses. Springer-Verlag, Berlin
Scranton R. et al., 2005, ApJ, 633, 589

Shankar F., Lapi A., Salucci P., De Zotti G., Danese L., 2006, ApJ, 643, 14
Smith D. J. B. et al., 2011, MNRAS, 416, 857
Smith D. J. B. et al., 2012, MNRAS, 427, 703
Swinbank A. M. et al., 2010, Nature, 464, 733
Wang L. et al., 2011, MNRAS, 414, 596
Wang Y., Brunner R. J., Dolence J. C., 2013, MNRAS, 432, 1961
Wardlow J. L. et al., 2013, ApJ, 762, 59
Xia J.-Q., Negrello M., Lapi A., De Zotti G., Danese L., Viel M., 2012, MNRAS, 422, 1324

[1] *Inst. de Fisica de Cantabria (CSIC-UC), Avda. los Castros s/n, E-39005 Santander, Spain*

[2] *SISSA, Via Bonomea 265, I-34136 Trieste, Italy*

[3] *Dipartimento di Fisica, Università di Roma 'Tor Vergata', Via Ricerca Scientifica 1, I-00133 Roma, Italy*

[4] *INAF–Osservatorio Astronomico di Padova, Vicolo dell'Osservatorio 5, I-35122 Padova, Italy*

[5] *Department of Physical Sciences, The Open University, Milton Keynes MK7 6AA, UK*

[6] *Sterrenkundig Observatorium, Universiteit Gent, Krijgslaan 281 S9, B-9000 Gent, Belgium*

[7] *Sydney Institute for Astronomy, School of Physics, University of Sydney, NSW 2006, Australia*

[8] *School of Physics and Astronomy, University of Nottingham, University Park, Nottingham NG7 2RD, UK*

[9] *Institute for Astronomy, University of Edinburgh, Royal Observatory, Blackford Hill, Edinburgh EH9 3HJ, UK*

[10] *Australian Astronomical Observatory, PO Box 915, North Ryde, NSW 1670, Australia*

[11] *Harvard–Smithsonian Center for Astrophysics, 60 Garden Street, Cambridge, MA 02138, USA*

[12] *Department of Physics and Astronomy, University of California, Irvine, CA 92697, USA*

[13] *International Centre for Radio Astronomy Research (ICRAR), University of Western Australia, Crawley, WA 6009, Australia*

[14] *Scottish Universities' Physics Alliance (SUPA), School of Physics and Astronomy, University of St Andrews, North Haugh, St Andrews, Fife KY16 9SS, UK*

[15] *Department of Physics and Astronomy, University of Canterbury, Private Bag 4800, Christchurch 8140, New Zealand*

[16] *School of Physics and Astronomy, Cardiff Univ., The Parade, Cardiff CF24 3AA, UK*

[17] *Instituto de Física y Astronomía, Universidad de Valparaíso, Avda. Gran Bretaña 1111, 2360102 Valparaiso, Chile*

[18] *European Southern Observatory, Karl-Schwarzschild-Str. 2, D-85748 Garching, Germany*

[19] *Astronomy Centre, University of Sussex, Falmer, Brighton BN1 9QH, UK*

[20] *Department of Physics and Astronomy, University of British Columbia, Vancouver, BC V6T 1Z1, Canada*

[21] *Key Laboratory of Particle Astrophysics, Institute of High Energy Physics, Chinese Academy of Science, PO Box 918-3, Beijing 100049, China*

This paper has been typeset from a TeX/LaTeX file prepared by the author.